Applied Surface Science 608 (2023) 155187

Contents lists available at ScienceDirect

Applied Surface Science

journal homepage: www.elsevier.com/locate/apsusc

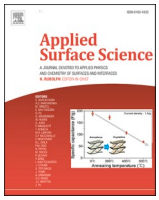

Full Length Article

Influence of hydrochloric acid concentration and type of nitrogen source on the electrochemical performance of TiO_2/N-MoS_2 for energy storage applications

Z. Zarach [a,*], A.P. Nowak [a,b], K. Trzciński [a,b], G. Gajowiec [c], G. Trykowski [d], M. Sawczak [e], M. Łapiński [b,f], M. Szkoda [a,b]

[a] Department of Chemistry and Technology of Functional Materials, Faculty of Chemistry, Gdańsk University of Technology, Narutowicza 11/12, 80-233 Gdańsk, Poland
[b] Advanced Materials Center, Gdańsk University of Technology, Gabriela Narutowicza 11/12, 80-233 Gdańsk, Poland
[c] Institute of Machine Technology and Materials, Faculty of Mechanical Engineering and Ship Technology, Gdansk University of Technology, Narutowicza 11/12, 80-233 Gdansk, Poland
[d] Faculty of Chemistry, Nicolaus Copernicus University, Gagarina 7, 87-100, Toruń, Poland
[e] Centre for Plasma and Laser Engineering, The Szewalski Institute of Fluid Flow Machinery, Fiszera 14, 80-231 Gdansk, Poland
[f] Institute of Nanotechnology and Materials Engineering, Faculty of Applied Physics and Mathematics, Gdańsk University of Technology, Narutowicza 11/12, 80-233 Gdańsk, Poland

ARTICLE INFO

Keywords:
Molybdenum sulfide
Titanium dioxide nanotubes
Nitrogen doping
Hydrochloric acid
Supercapacitors
Energy storage

ABSTRACT

In this work, nitrogen-doped molybdenum sulfide was directly deposited on titanium dioxide nanotubes substrate (TiO_2/N-MoS_2) during hydrothermal synthesis. The study focuses on the influence of hydrochloric acid concentration used for the synthesis, with the results indicating its essential role in thioacetamide hydrolysis and thus in the effectiveness of the N-MoS_2 deposition. The electrode material itself is characterized by an initial capacitance of 320 mF cm^{-2} with 76 % capacitance retention after 10 000 cycles. Moreover, the effect of nitrogen source on the physical and capacitive properties is investigated, revealing that the simultaneous addition of aniline and ammonium persulfate contributes to the improvement of crystallinity and overall electrochemical performance of the electrode material. The analysis of charge storage mechanisms also indicates that the introduction of nitrogen atoms significantly affects the contribution of diffusion-controlled processes. In the construction of a symmetrical device, the specific capacitance of 76 F g^{-1} and areal capacitance of 70 mF cm^{-2} with the superior coulombic efficiency and 84 % of capacitance retention after 15,000 cycles is observed, with 11.1 W kg^{-1} and 5193.4 Wh kg^{-1} of energy and power density of the device, respectively.

1. Introduction

Nowadays, supercapacitors, also known as electrochemical capacitors, are one of the key elements of energy management systems, mainly due to their high-power density, but also because of the possibility of integrating them with energy conversion devices [1]. In addition to their ever increasing use in electric vehicles [2,3], they are also attracting attention for their use in portable and wearable electronics [4–6]. Furthermore, in order to constantly improve their properties, primarily related to the improvement of the energy density and the expansion of the device operation voltage, new electrode materials are still being sought, as they are one of the key elements affecting the overall electrochemical performance.

In the case of electrode materials for supercapacitors, the most commonly used are carbonaceous ones, such as graphene, carbon nanotubes and porous carbons of different types [7]. Carbon electrodes store the charge mainly through an electrical double layer (EDL), which is formed when a potential is applied to the electrode and the ions adsorb on the surface. This group of electrode materials is one of the mostly studied, as they possess a high specific surface area and a high porosity which facilitates the diffusion of the charged species [8]. Furthermore, 2D materials like graphene have been receiving a considerable attention, mainly due to its two-dimensional structure and hence the possibility of a large surface area accessibility, as well as its mechanical and electronic properties [8–10]. Especially in the case of both Na- and Li-ion batteries, expanding the spacing between graphene/graphite

* Corresponding author.
E-mail address: zuzanna.zarach@pg.edu.pl (Z. Zarach).

https://doi.org/10.1016/j.apsusc.2022.155187
Received 2 August 2022; Received in revised form 26 September 2022; Accepted 30 September 2022
Available online 7 October 2022

layers enables efficient energy storage [11]. It is the two-dimensional structure that is one of the properties that draws the attention in the relation to energy storage materials. Among these 2D structures, apart from carbon ones, materials such as MXenes [12,13], transition metal oxides and phosphates [14–17], but also transition metal dichalcogenides (TMDs) are of particular interest.

TMDs is a group of layered materials that are characterized by the X-M−X structure, composed of transition metals (M) and chalcogens (X). Materials from this group like MoS_2, WS_2, VS_2 and $MoTe_2$ [18–21], recently are gaining more and more interest in terms of their application in energy storage, mainly due to their properties such as edge sites, large specific surface area and ease of intercalation [22]. Special attention is paid to MoS_2, which seems to be the most thoroughly studied one, however, due to the variety of synthesis methods and attempts to deposit MoS_2 on various substrates, there is still no systematic knowledge about the correlation between material properties and synthesis parameters, and many other questions related to this arise, for which the answer still remains open. Nowadays, an increasingly widely used approach is hydrothermal synthesis, which offers a fast and low-cost procedure for obtaining nanostructured 2D TMDs. MoS_2 synthesized by hydrothermal method in the form of various structures such as: nanosheets [23], nanospheres [24], nanowires [25], nanorods [26], or hollow nanoparticles [27] has been repeatedly reported in the literature. However, due to the diverse selection of precursors, solvents and additives, as well as the inability to precisely control the processes taking place in the hydrothermal vessel, the MoS_2 crystal growth mechanism and the influence of individual parameters on the final properties of the material are not entirely clear. One of the most frequently chosen solvents in hydrothermal synthesis is deionized water [28–30], but an aqueous solution of hydrochloric acid [31–33] or organic solvents [34,35] are reported, and each of them plays an essential role in the final properties of the material. Therefore, the crucial aspect of hydrothermal synthesis is to understand the importance and the influence of each parameter on material's growth mechanism. However, as far as authors are concerned, so far there was no investigation on the impact of HCl concentration on the physical and electrochemical properties of MoS_2 altogether with its energy storage abilities.

In general, when it comes to electrode materials for energy storage, apart from investigating the influence of individual synthesis parameters, a number of studies are carried out in order to improve the capacitive properties of the materials. Among such solutions, the aim is to synthesize materials in the nanoscale and, above all, to create hybrid electrode materials. TMDs are commonly combined with conductive polymers [36,37], carbon materials [38,39], or MXenes [40], which results in increased energy density and enhanced stability of electrode within charge–discharge cycles. The improvement of electrochemical properties, and in particular the improvement of material's conductivity, is also performed by doping TMDs with various metal atoms, including: nitrogen [28,41,42], cobalt [43], platinum [44], or copper [45]. Moreover, material doping may also lead to imperfections due to atomic rearrangement and thus results in creating more active sites [45].

When it comes to materials used for energy storage, not only should the capacitive properties be considered, but also the material's interaction with the current collector at the interface. The most common practice is the synthesis of materials in the form of powders altogether with the polymer binders application for connecting the active material with the current collector. Unfortunately, binders application contributes to an increase in resistance and reduction of the positive effect caused by the formed nanostructures. Therefore, obtaining materials directly on the conductive substrates is one of the steps to improve the electrochemical performance of energy storage materials. In the case of MoS_2, only few papers have been reported about the synthesis of electrode materials performed in this way [46–49]. However, a major limitation is the fact that most of them require advanced equipment or/and hard synthesis conditions, and thus an efficient, low-cost, and scalable synthesis technique is still being sought.

In this work, we present a facile hydrothermal synthesis of nitrogen-doped molybdenum sulfide (N-MoS_2) performed directly on TiO_2 nanotubes substrate with a thorough investigation of the influence of hydrochloric acid concentration on the physical and electrochemical properties of the electrode material. Furthermore, the effect of the addition of aniline and ammonium persulfate during the synthesis was studied, with the results indicating that their presence significantly enhanced the capacitive properties of the electrode material. The resulted TiO_2/N-MoS_2 electrode material was characterized by the initial capacitance of 320 mF cm^{-2}, and the improved electrochemical performance was achieved mainly through adjusting concentration of hydrochloric acid and introducing nitrogen atoms into MoS_2 structure. Furthermore, TiO_2/N-MoS_2 material was used to construct a symmetrical device, for which the obtained specific capacitance reached 76F g^{-1} (C_{areal} = 70 mF cm^{-2}), with energy density of 11.1 W kg^{-1} and superior power density (5193.4 Wh kg^{-1}).

2. Materials and methods

2.1. Materials

In the anodic oxidation process titanium foil (0.127 mm thick, annealed, 99 %), purchased from Alfa Aesar, was used and the synthesis was preceded by a sonication procedure using acetone and isopropanol mixture (Chempur). The electrolyte consisted of reagents from Chempur: ammonium fluoride (NH_4F) pure p.a., ethylene glycol ($C_2H_6O_2$), phosphoric acid (H_3PO_4), and distilled water. Hydrofluoric acid used for etching was purchased from Fischer Chemical. Reagents used for the hydrothermal process: potassium molybdenum oxide, anhydrous (99.8 % metals basis, Alfa Aesar), thioacetamide (Chemat), ammonium persulfate (APS) (98 %, Sigma-Aldrich), and aniline (ANI) (99.8 % pure, Acros Organics) were all at pure analytical grade. Sulfuric acid (POCH) was used for electrochemical measurements and as an electrolyte in supercapacitor construction. The device was constructed using heat-sealable foil and a fiberglass separator using a vacuum packing machine (CAS CVP-350/MS, Hertogenbosch).

2.2. TiO_2 nanotubes synthesis

Titanium dioxide nanotubes (TiO_2 NTs) were prepared by applying an anodic oxidation procedure according to our previous report [50]. In short, titanium foil was cut into pieces (2 cm × 2 cm), cleaned using ultrasonic treatment in isopropanol: acetone mixture (1:1 v/v) for 20 min, and rinsed with distilled water eventually. The as-prepared Ti foil constituted a working electrode (WE) and another Ti foil as a counter electrode (CE) in a two-electrode configuration in the anodization process. The synthesis was carried out at a constant temperature (23 ℃) using a cooling bath thermostat (KISS K6, Huber), with a voltage of 40 V applied for over 2 h. After that, the electrode was rinsed with distilled water and etched by immersing in HF several times. In the final step, the electrode was calcinated in the quartz tube furnace through heating up to 450 ℃ in 2 h, sintering at this temperature for 2 h and 45 min.

2.3. TiO_2/N-MoS_2 preparation

TiO_2/N-MoS_2 was obtained by hydrothermal synthesis. For this purpose, 0.5 g of potassium molybdate and 1 g of thioacetamide were diluted in 25 ml of 0.5 M HCl and stirred for 10 min. Subsequently, 63 mg of aniline (26 mM) and 153 mg ammonium persulfate (26 mM) were added and stirred for another 20 min. Finally, the mixture was transferred to the Teflon liner altogether with the TiO_2 NTs sample (inside of a stainless steel autoclave) and placed in an oven for 24 h at 200 ℃. After the process, the TiO_2/N-MoS_2 electrode was rinsed with distilled water and dried at room temperature. In order to investigate the effect of the hydrochloric acid concentration, it was changed from 0.1 to 5 M, respectively.

2.4. Electrochemical measurements

Electrochemical measurements were performed using potentiostat/galvanostat (BioLogic VSP 2078) in a three-electrode configuration – platinum mesh constituted a counter electrode (CE), Ag/AgCl vs 3 M KCl worked as a reference electrode (REF) and TiO_2/N-MoS_2 was a working electrode (WE). Measurements were carried out in 1 M sulfuric acid (H_2SO_4) aqueous solution and a number of electrochemical techniques have been applied, e.g. cyclic voltammetry (CV), galvanostatic charge and discharge tests (GCD), and electrochemical impedance spectroscopy (EIS). EIS was performed in a frequency range between 20 kHz and 100 mHz with a voltage amplitude of 10 mV. The impedance of the constant phase element Q used in the model is represented by the Equation below:

$$Z(\omega) = P^{-1}(j\omega)^{-n} \quad (1)$$

In order to investigate the performance in a two-electrode configuration, a symmetric supercapacitor was constructed using two TiO_2/N-MoS_2 electrodes. The total mass loading in the supercapacitor construction was 1.83 mg. Electrodes were separated using a fiberglass separator soaked in 1 M H_2SO_4 electrolyte and they were encased with a heat-sealable foil using a vacuum packing machine.

2.5. Material characterization

The as-prepared electrode materials were characterized by microscopic techniques, including Scanning Electron Microscopy (SEM) using JSM-7800F (JEOL, Tokyo, Japan) field emission scanning electron microscope. The images were analyzed using a beam accelerating voltage at 5 kV. EDX analysis was performed with a silicon nitride window's detector (OCTANE ELITE model, EDAX company, Mahwah, NJ, USA), and Transmission Electron Microscopy (TEM) (FEI, Tecnai F20X-Twin) with the measurement parameters: voltage 200 kV from FEG, imaging in bright field (BF) with CCD camera (Gatan, Orius), vacuum in the chamber 10^{-4} Pa. Raman spectroscopy measurements were performed with a micro-Raman spectrometer (Renishaw InVia) operating at 1 % of its total power (50 mW), with Ar laser emitting at the wavelength of 514 nm. X-ray Photoelectron Spectroscopy was carried out with an X-ray photoelectron spectrometer (Argus Omicron NanoTechnology) with Mg-Kα source of X-ray and anode operated at 15 keV, 300 W. XPS measurements were conducted under ultra-high vacuum at room temperature, with pressure below 1.1×10^{-8} mbar. XRD analysis was done with a diffractometer (Xpert PRO-MPD) with Cu Kα emission (λ = 0.15406 nm).

3. Results and discussion

3.1. Characterization of the TiO_2/N-MoS_2 electrode materials prepared with different HCl concentrations

Electrode materials obtained with different hydrochloric acid concentrations were investigated using Scanning Electron Microscopy (SEM) and the results are presented in Fig. 1, indicating that the concentration significantly influenced the morphology of the samples. When the concentration was low (0.1 and 0.2 M), the formation of nanostructures was not observed, whereas, for the highest HCl concentration, nanostructures in a form of cubes and spheres may be distinguished. However, according to the results of Raman spectroscopy and XPS analysis, it may be assumed that the cubes and spheres formation is not due to the MoS_2 synthesis, but is strictly related to the change in the structure of TiO_2 nanotubes, which was caused by the treatment with 5 M HCl. According to some literature reports, treatment of TiO_2 nanotubes with HCl may considerably affect the shape of nanotubes, but the pH value may have some impact on crystallinity and morphology, as well [51–53]. Furthermore, Fan et al. also pointed out that the treatment of carbon nanotubes with hot concentrated HCl led to the formation of closed-capped nanotubes [54]. The closing of TiO_2 NTs was confirmed by the cross-section image and EDS analysis for the 5 M sample (see Figs. S1 and S2**a**), which clearly shows that the composition is only titanium and oxygen, as well as that the tip of the nanotube has been transformed into a cube, cutting off access to the inside of the nanotubes.

The enhanced signal from titanium was also reported for the sample with 3 M HCl (Fig. S2**b**), indicating that the synthesis of MoS_2 was also not fully effective. However, one may see that the resulting morphology for 0.5 and 1 M samples of TiO_2/N-MoS_2 is fairly similar, as the structure of nanosheets may be observed for both of them. Furthermore, for both of them, the EDS analysis confirmed the presence of elemental Mo and S in the deposited layers (see Fig. S2**c,d**). The SEM results are consistent with the morphology that can be seen in the transmission electron microscopy (TEM) images (see Fig. 2). TEM measurements were performed for the precipitate that was formed during the synthesis. It is impossible to indicate the presence of nanostructures for the samples prepared with 0.1 M and 0.2 M HCl, however, the 0.2 M sample is noticeably more

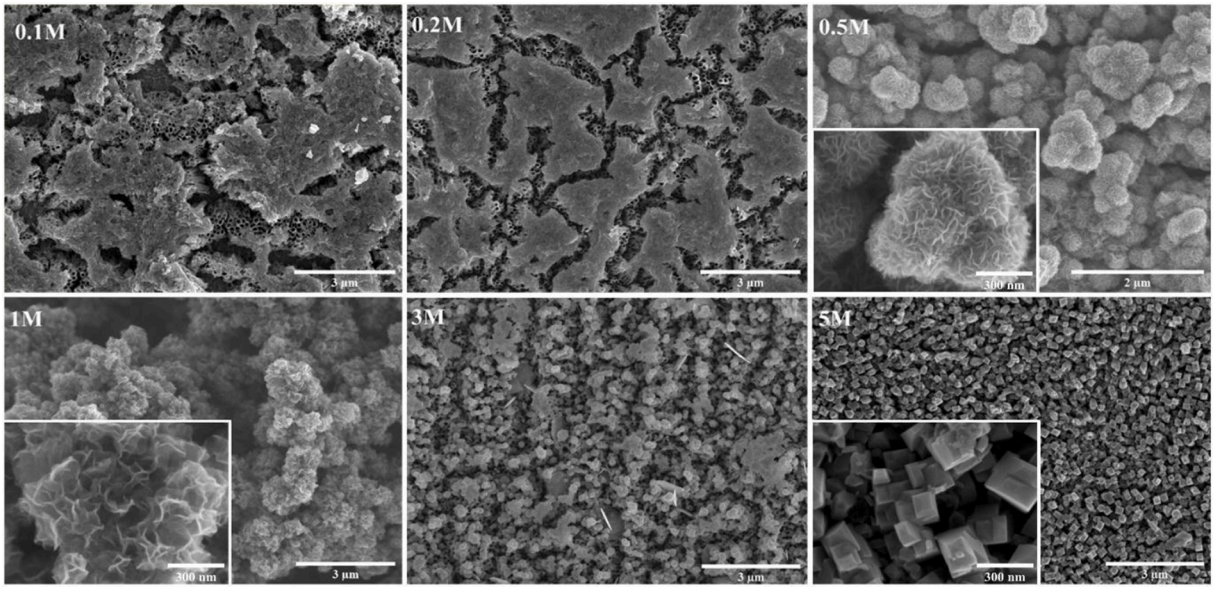

Fig. 1. SEM images of TiO_2/N-MoS_2 electrode materials obtained after hydrothermal synthesis performed with different hydrochloric acid concentrations.

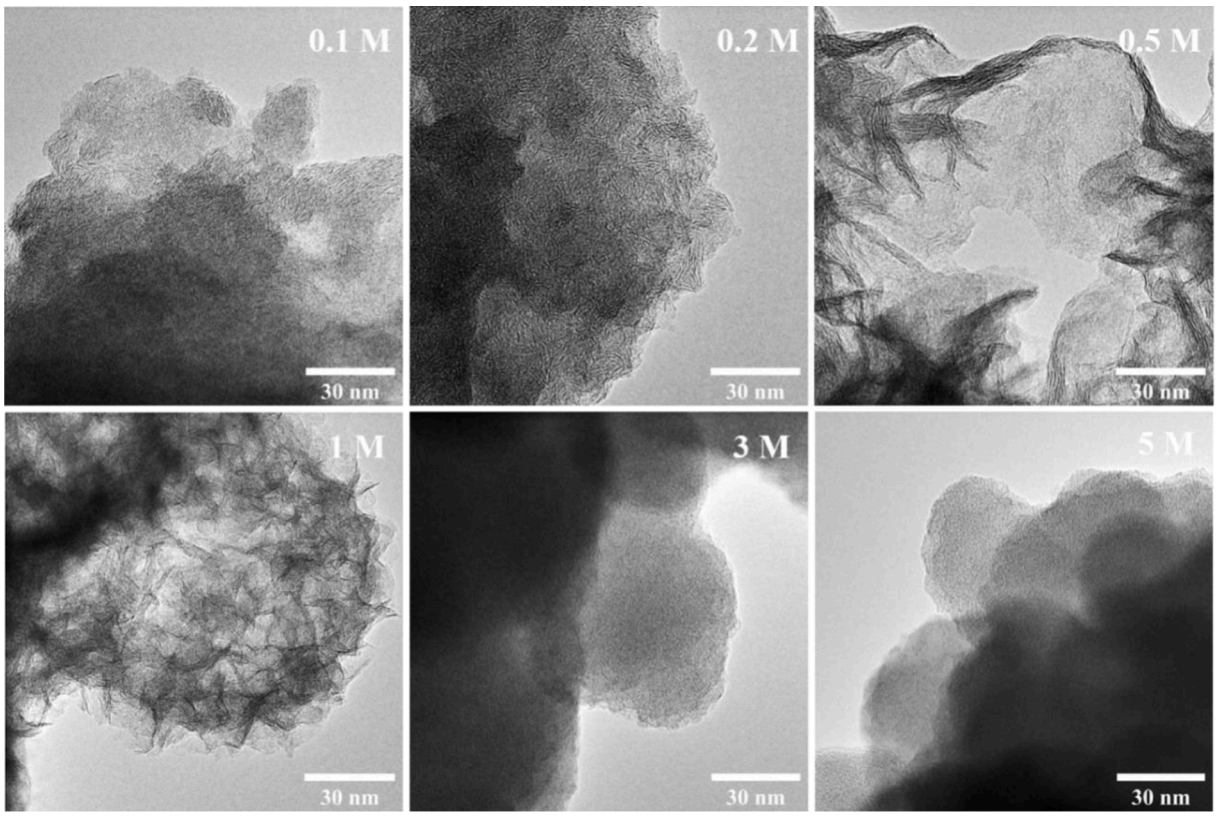

Fig. 2. TEM images of TiO_2/N-MoS_2 electrode materials obtained after hydrothermal synthesis performed with different hydrochloric acid concentrations.

crystalline. The crystal structure is also clearly distinguishable with 0.5 M and 1 M materials, especially at the edges of the nanosheets, whereas materials prepared with the highest HCl concentration are mostly amorphous. These results were also confirmed by the XRD results, presented in Fig. 3. Despite the fact that the results mainly show signals from Ti/TiO_2 substrate, it is possible to extract the signals from molybdenum sulfide, as well. Peaks typical for the hexagonal structure of MoS_2 may be indicated, including ones at 32.48° and 57.31° corresponding to (1 0 0) and (1 1 0) planes, respectively [55]. However, the signals are visible only for the materials prepared with 0.2 M, 0.5 M, and 1 M hydrochloric acid, with the highest intensities of the peaks recorded for the 0.5 M HCl sample. Among other signals coming from the substrate, one can distinguish signals of titanium at 40.36° and 53.15° for (1 0 1) and (1 0 2) planes, respectively [56]. Moreover, several signals

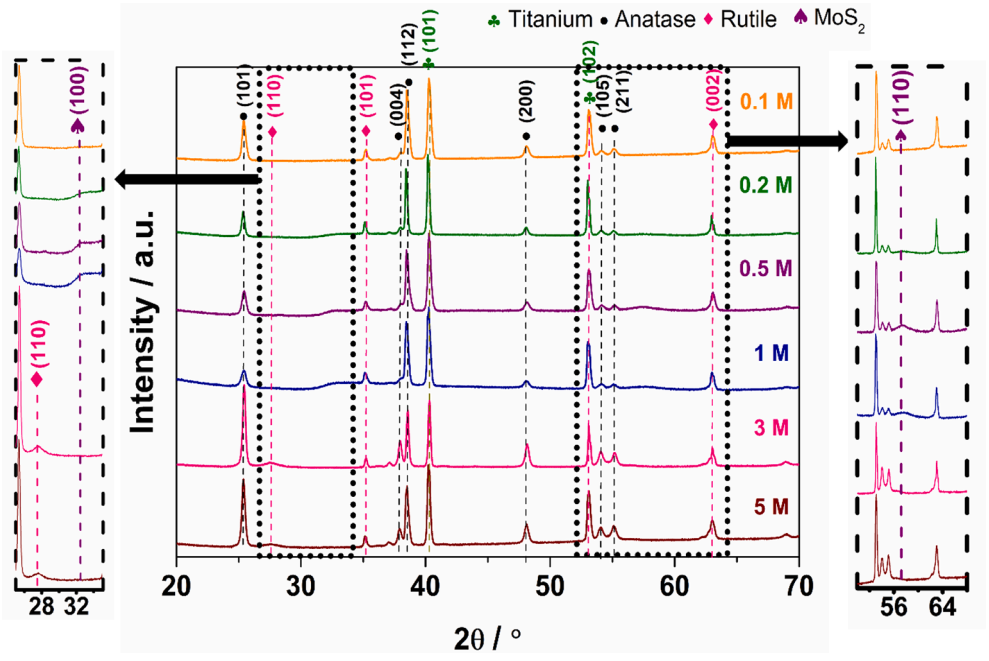

Fig. 3. XRD results for TiO_2/N-MoS_2 electrode materials obtained after hydrothermal synthesis performed with different hydrochloric acid concentrations.

from the anatase phase of TiO_2 were recorded, including 25.42°, 38.03°, 38.70°, 48.05°, 54.15°, and 55.15° corresponding to (101), (004), (112), (200), (105) and (211) planes, respectively [57]. Also, the presence of a rutile phase was confirmed, especially for the samples treated with high concentration hydrochloric acid. It was shown recently that the HCl environment enhances the anatase to rutile transition [58], which is probably even more triggered when the concentration is increased.

On this basis, it may be concluded that the synthesis of MoS_2 was strictly dependent on the hydrochloric acid concentration, as the deposition was effective only when the concentration was moderate (0.2 – 1 M). The conclusions were also based on Raman spectroscopy results (see Fig. S3**a**), for which one may see the presence of a hexagonal phase of MoS_2, confirmed by the presence of peaks at 376 cm^{-1} and 404 cm^{-1}, attributed to the vibrations in 2H-MoS_2 molecules, namely E^1_{2g} in-plane and A_{1g} out-plane active modes, respectively [59,60]. However, with both decreased and increased concentration, the synthesis was not effective as only the signals characteristic for TiO_2 may be distinguished. To further verify the presence of the synthesized MoS_2 and the nitrogen dopant, the XPS analysis was applied.

The results of the XPS analysis are presented in Fig. 4. The results indicate, that even for the materials prepared with the lowest and the highest hydrochloric acid concentration, some amount of molybdenum in the form of Mo^{4+} and Mo^{6+}, as well as sulfur, may be detected. However, in the case of the 3 M HCl sample, the signal mainly comes from the trigonal phase of molybdenum sulfide, whereas for the highest HCl concentration, the most intense signal is due to the presence of Mo^{6+}, and stoichiometry does not indicate the presence of molybdenum sulfide. Nevertheless, for the moderate acid concentration, two signals at 227.9 and 231.1 eV suggest the presence of the trigonal phase (1T) of MoS_2, whereas the existence of the 2H phase is confirmed by the signals recorded at 228.9 and 232.2 eV [59,60]. Analogously, one can distinguish between signals recorded for sulfur – the values of the S $2p_{1/2}$ and $2p_{3/2}$ signals from 2H and 1T phases are placed at 161.8 and 163.6 eV, and 161.3 and 163.3 eV, respectively [61,62]. Furthermore, XPS spectra reveal the presence of SO_4^{2-}, which may be related to the presence of synthesis residues, but also the S^{2-} conversion [63]. For most of the samples, the XPS profile of the N1 s consists of the band at 394.3 eV, assigned to Mo $3p_{3/2}$, as well as two bands N1 at 399.5 eV and N2 at 397.0 eV, which resulted from nitrogen presence in the samples. The N1 signal is related to the presence of non-charged nitrogen, ascribed to the N—C bonding. On the other hand, the signal designated as N2 indicates the presence of negatively charged nitrogen resulting from Mo–N bonding [64]. Comparing the results obtained for different HCl concentrations, it may be stated that the 0.5 M and 1 M samples are characterized by the highest nitrogen content, and the difference is particularly clear due to the higher intensity of the N1 signal. The atomic percentage of nitrogen estimated from XPS analysis, % ratio of both N1 to N2 and total N to Mo is presented in **Table S1**.

3.2. *Electrochemical measurements for TiO_2/N-MoS_2 electrode materials prepared with different HCl concentrations*

For the evaluation of the electrochemical properties, electrode materials synthesized with various HCl concentrations were investigated in 3-electrode configuration in 1 M H_2SO_4. Firstly, using cyclic voltammetry, the potential range within which electrode materials are capable of charge storage was determined and the results are presented in Fig. 5**a**. It turned out that TiO_2/N-MoS_2 electrode materials obtained with both 0.5 M and 1 M HCl were characterized by the best capacitive properties, which can be observed in the cyclic voltammetry curves. It was also confirmed during galvanostatic charge and discharge measurements (see Fig. 5**b**) – the results show that for the TiO_2/N-MoS_2 electrode material synthesized with 0.5 M HCl, the areal capacitance value was the highest, which was indicated by the initial capacitance of 320 mF cm^{-2}, as well as it was characterized by better capacitance retention after 1000 cycles in comparison with other materials. It is worth mentioning that the deposited MoS_2 layer was not very thick at all, (which could be the cause of such improved capacitance value), and despite its unevenness, it was only up to several micrometers at its thickest point (see Fig. S3**b**). Therefore, for the TiO_2/N-MoS_2 electrode material presenting the best capacitive properties, a further study on the

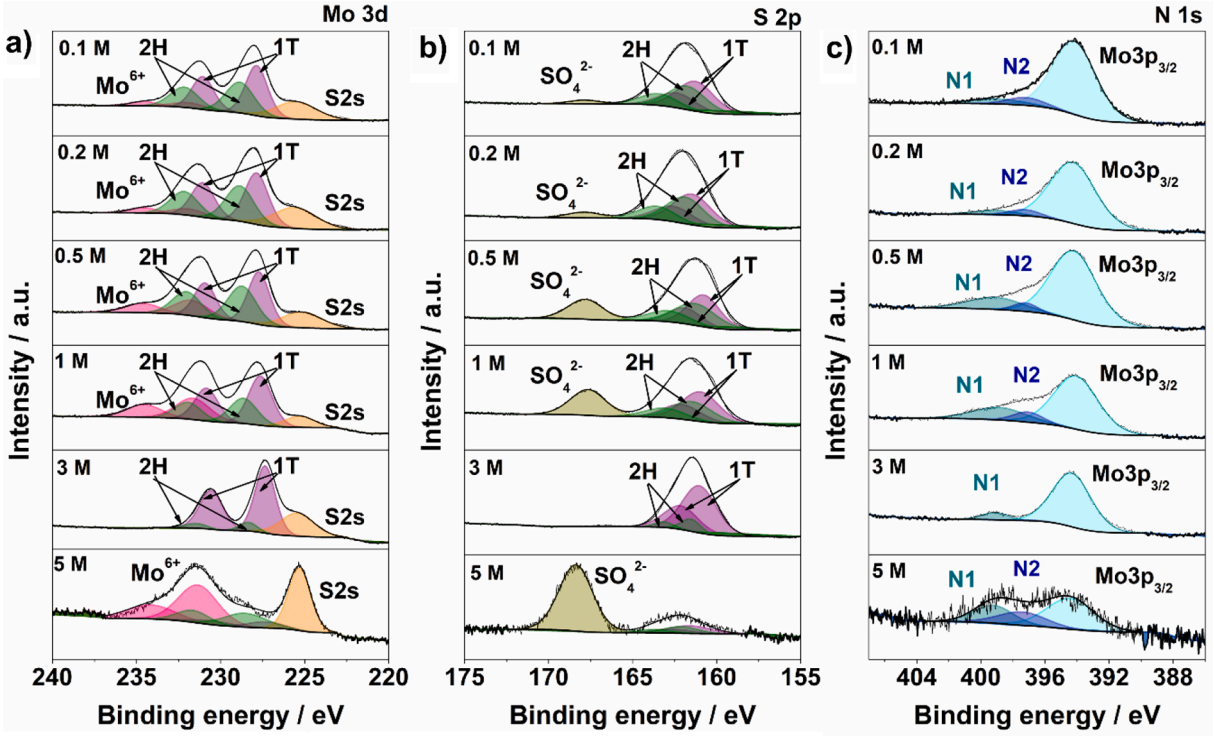

Fig. 4. XPS results for TiO_2/N-MoS_2 electrode materials obtained after hydrothermal synthesis performed with different hydrochloric acid concentrations.

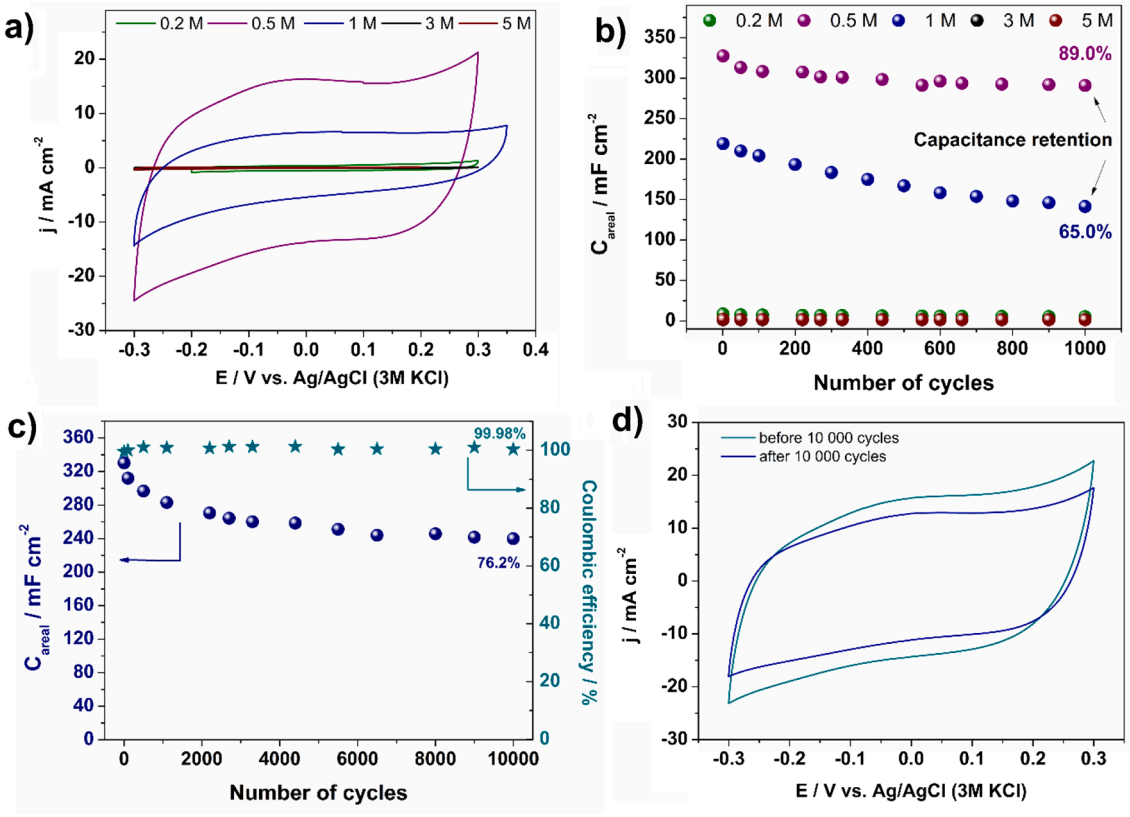

Fig. 5. a) CV curves (v = 50 mV s^{-1}) recorded in 1 M H_2SO_4 for TiO_2/N-MoS_2 electrode materials prepared with various HCl concentrations; b) Areal capacitance value during 1000 cycles, calculated on the basis of GCD tests; c) Areal capacitance and coulombic efficiency for TiO_2/N-MoS_2 (0.5 M) electrode material during 10 000 GCD cycles; d) CV curves for TiO_2/N-MoS_2 (0.5 M) before and after 10 000 GCD cycles.

ability of energy storage was conducted. After 10000 galvanostatic charge–discharge cycles, electrode material was characterized by the areal capacitance of 240 mF cm^{-2}, with the coulombic efficiency of around 99.98 % (see Fig. 5**c**). Moreover, the shape of the cyclic voltammetry curve after galvanostatic tests indicates that despite the loss of some capacitance, the material is still capable of charge storage.

3.3. The influence of HCl concentration on the growth of MoS_2 on TiO_2 nanotubes substrate

MoS_2 synthesis using the hydrothermal method has been repeatedly reported in the literature, however, the mechanism of molybdenum sulfide crystal growth in solution still remains an open question. In order to explore this issue, the influence of hydrochloric acid concentration on the properties of the obtained MoS_2 layer was analyzed, and the possible course of the reaction was proposed. The synthesis of molybdenum sulfide begins with the hydrolysis of thioacetamide, and this process can be efficiently catalyzed and accelerated through the acidic reaction medium [65–67], and the obtained hydrogen sulfide forms the following equilibrium when dissolved in water:

$$C_2H_5NS + H_2O\,H^+ \rightarrow CH_3COOH + H_2S + NH_3 \quad (2)$$

$$H_2S_{(aq)} \leftrightarrow H^+_{(aq)} + HS^-_{(aq)} \quad (3)$$

$$HS^- \leftrightarrow H^+ + S^{2-} \quad (4)$$

The hydrogen sulfide obtained in the reaction is the main source of sulfur in the further synthesis process, and acts as a reducing agent that reacts with the molybdenum precursor present in the solution [68]:

$$4\,MoO_4^{2-} + 9\,H_2S + 6\,CH_3COOH \rightarrow 4\,MoS_2 + SO_4^{2-} + 6\,CH_3COO^- + 12\,H_2O \quad (5)$$

When hydrochloric acid was not present during the synthesis, no formation of nanostructures was observed, and the electrochemical properties of the material were insufficient (see **Figure S4**). Similar observations were made for the synthesis with low concentrations of hydrochloric acid, but increasing its concentration to 0.5 M resulted in a significant improvement in the material's capacitive properties, and the formation of nanosheet structures was observed, which is attributed to the increased amount of H_2S, and thus the accelerated reaction of thioacetamide hydrolysis in a more acidic environment. Furthermore, according to the TEM measurements, it may also be concluded that all together with the increasing HCl concentration, the crystallinity of the MoS_2 was improved, and similar observations were reported by Matsui et. al for the ZrO_2 synthesis [69], as well as by Li et al. for the perovskites synthesis [70], with pointing out the fact that the concentration of H^+ ions significantly affects the single particle size. However, no further enhancement in electrochemical properties was observed with increasing acid concentration. The reason for such a phenomenon may be the unfavorable interference of HCl with the substrate material – TiO_2 nanotubes. As the results presented above show, high concentrations of HCl not only changed the surface of the nanotubes but also contributed to the formation of an additional TiO_2 crystal phase (rutile). As a result, it hindered the effective deposition of molybdenum sulfide on the substrate, and the effect was intensified with an increase in the acid concentration.

3.4. The role of aniline (ANI) and ammonium persulfate (APS) in the hydrothermal synthesis of TiO_2/N-MoS_2

During the simultaneous synthesis and deposition of molybdenum sulfide on TiO_2 substrate by hydrothermal method, apart from precursors of molybdenum and sulfur, aniline and ammonium persulfate were added. According to the literature, the synthesis of molybdenum

sulfide altogether with polyaniline, commonly with the assistance of hydrothermal synthesis, is frequently reported [71–76] and considered successful. The presented synthesis was also initially aimed at obtaining a layer of a hybrid MoS_2/PANI electrode material, deposited on a TiO_2 substrate. However, the results of the solid-state physics analysis do not indicate the presence of polyaniline in the electrode material. Moreover, the results obtained using cyclic voltammetry also do not evidence that polyaniline was effectively deposited on the TiO_2 substrate (see Fig. 5**a**), as characteristic peaks related to the polyaniline redox reactions [77] can't be distinguished. Unexpectedly, when aniline and ammonium persulfate were excluded from the synthesis, the electrode material lost a significant part of its capacitive properties, which is presented in Fig. 6**a**. On the basis of the cyclic voltammetry results, it may be concluded that the addition of aniline or ammonium persulfate separately caused a similar effect and the presence of both during synthesis somehow contributes to improved electrochemical performance. In order to investigate the differences between the electrode materials and reveal the reason for the improved charge storage ability with the ANI and APS addition, scanning electron microscopy was used for the morphology study, and the results are presented in Fig. 6**b**. Each synthesis was conducted with a 0.5 M hydrochloric acid concentration. For the electrodes prepared with aniline and APS, the structure of the nanosheet is observed, but in general, they look quite alike. One may say that the structure of the nanosheets is more developed, especially in the presence of both ANI and APS, and what was pointed out by TEM measurements is that at the edges of these structures a crystalline form is observed in particular. Moreover, although Raman spectroscopy (Fig. 6**c**) showed no significant changes in the composition, only confirming the presence of the 2H MoS_2 phase in each electrode material, XRD analysis indicated some differences. XRD measurements were performed on the layer scraped off the TiO_2 substrate in order to further analyze the properties of the deposited layer. As presented in Fig. 6**d**, when ANI and APS were added during the synthesis, some characteristic diffraction peaks at 12.85°, 32.30°, 35.44°, and 57.04° may be distinguished that could be assigned to (0 0 2), (1 0 0), (1 0 2) and (1 1 0) planes oh hexagonal phase of MoS_2, respectively (JCPDS No. 37–1492). Also, two more diffraction peaks at 28.28° and 43.11° with considerably lower intensities are visible, corresponding to the (0 0 4) and (0 0 6) planes [55]. However, when the additional reagents were not included in the synthesis, a decrease in the intensity of the diffraction peaks was observed, especially when both of them were not present. The results indicate that the addition of aniline and ammonium persulfate may significantly influence the crystallinity of the MoS_2 layer.

To further evaluate the differences between the electrode materials, XPS analysis was performed with the recorded spectra shown in Fig. 7. The results are consistent with the ones obtained from other techniques, indicating the presence of both hexagonal and trigonal phases of molybdenum sulfide (see Fig. 7**a**). Moreover, for each sample, a small amount of molybdenum in a 6 + oxidation state was detected, probably related to the sample oxidation upon the air. Sulfur was also identified in each electrode material (see Fig. 7**b**), with trace amounts of SO_4^{2-}, which can be related both to the presence of synthesis residues, but also the S^{2-} conversion [63]. Most informative are the results for the region of nitrogen binding energy, presented in Fig. 7**c**. It may be observed that when aniline and ammonium persulfate were not present during the synthesis, the XPS profile of the N1 s mainly consists only of the band at 394.3 eV, assigned to Mo $3p_{3/2}$, with a weak signal at 397.0 eV indicating the presence of negatively charged nitrogen resulted from Mo–N bonding. On the other hand, the band at 399.5 eV is only recognizable for the sample with both ANI and APS, indicating that in this case, the doping process was most successful.

The investigation of the influence of both aniline and ammonium persulfate was also evaluated for the impact on the mechanism by which energy storage takes place. Pseudocapacitance is frequently associated with surface redox reactions, however, these reactions usually take place not only at the interface between electrode and electrolyte but also throughout the electrode material, altogether with reversible insertion of charge balancing ions [78]. According to Trasatti's approach [79], it is possible to estimate the contribution of the "outer" and "inner" surface of the electrode in energy storage processes, using Eq. (6):

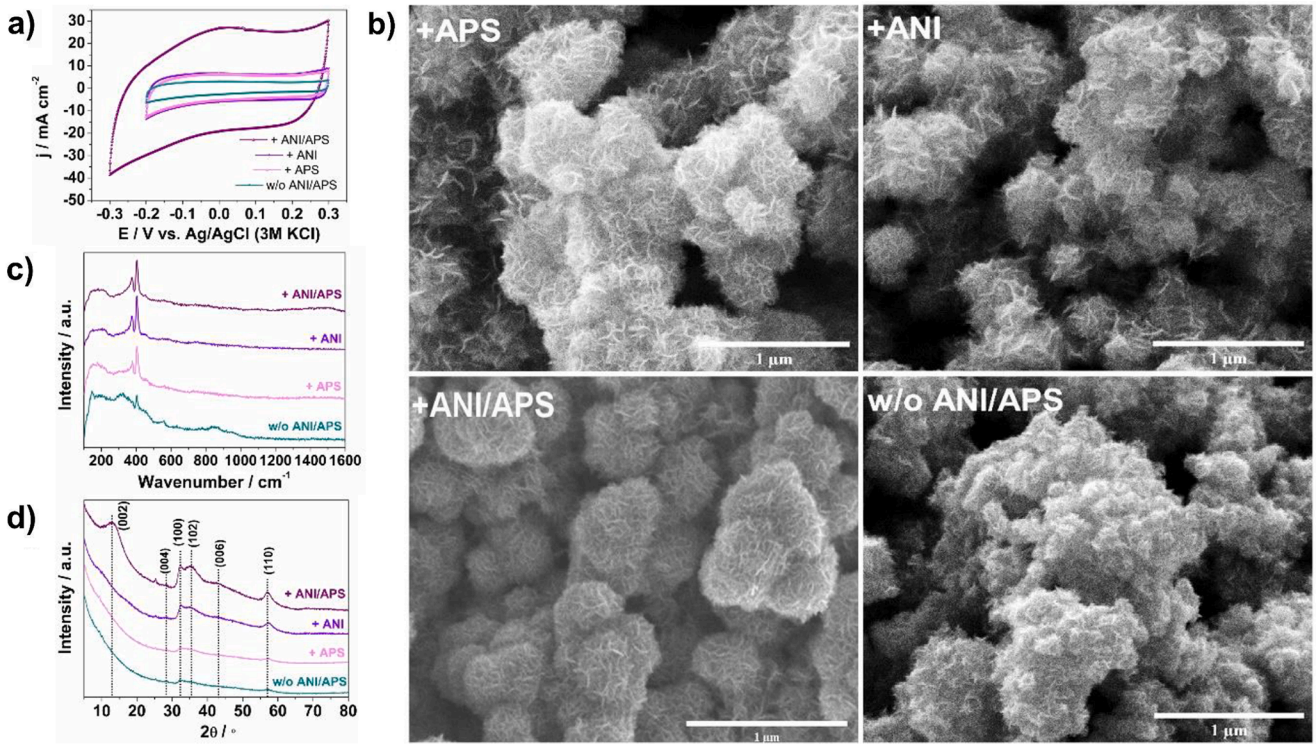

Fig. 6. a) CV curves (v = 50 mV s^{-1}) recorded in 1 M H_2SO_4, b) SEM images, c) Raman spectroscopy and d) XRD results for TiO_2/N-MoS_2 and TiO_2/MoS_2 electrode materials prepared with and without the addition of aniline and ammonium persulfate during synthesis, respectively (with 0.5 M HCl).

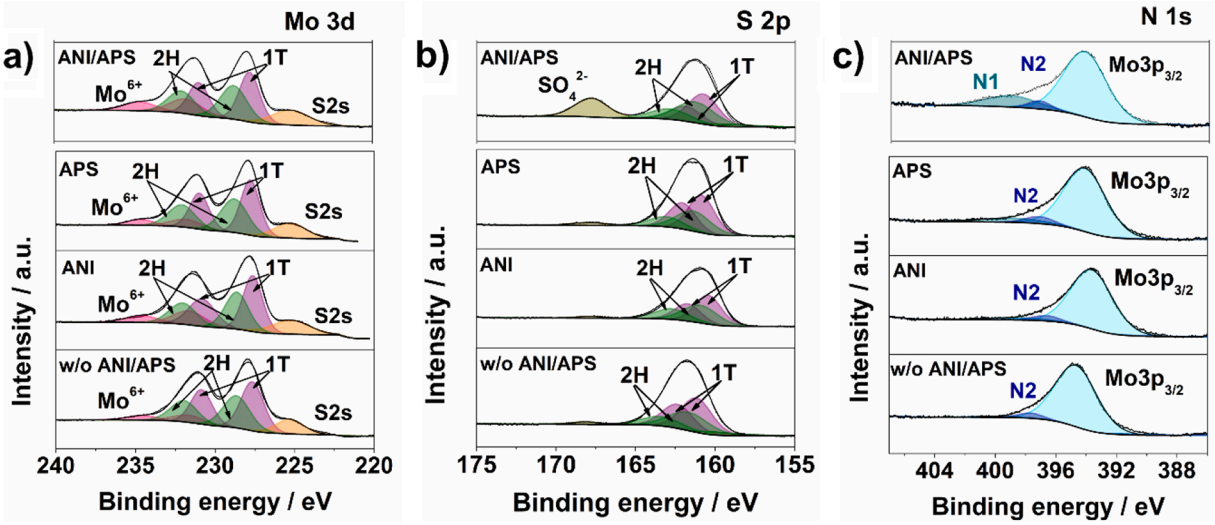

Fig. 7. XPS spectra of a) Mo3d, b) S2p and c) N1s for TiO_2/N-MoS_2 and TiO_2/MoS_2 electrode materials prepared with and without the addition of aniline and ammonium persulfate during synthesis (with 0.5 M HCl).

$$q_T = q_i + q_o \tag{6}$$

where q_T represents the total amount of charge, q_i stands for the charge at the inner surface and q_i represents the charge stored at the "inner" surface and q_o is related to the charge stored at the outer surface. After cyclic voltammetry measurements at different scan rates, a linear relationship between the reciprocal of the calculated areal capacitance (C^{-1}) and the square root of the scan rate (see Eq. (7)):

$$C^{-1} = \text{const} \bullet v^{1/2} + C_T^{-1} \tag{7}$$

C_T corresponds to the sum of both "outer" and "inner" capacitance. Eventually, the dependence between the capacitance and the reciprocal of the scan rate enables estimating the contribution of the "outer" layer (C_O), according to Eq. (8):

$$C = \text{const} \bullet v^{-1/2} + C_O \tag{8}$$

On the other hand, Conway's approach [80], modified by Dunn et al. for nanostructured transition metal oxides, is based on the statement that the total current response is the sum of the current related to the diffusion-limited and surface-controlled processes:

$$i(V) = k_1 v + k_2 v^{1/2} \tag{9}$$

The linear dependence between the slope (k_1) and Y-intercept (k_2) allows for determining the contribution of both surface-confined and diffusion controlled processes to the total charge being stored:

$$\frac{i(V)}{v^{1/2}} = k_1 v^{1/2} + k_2 \tag{10}$$

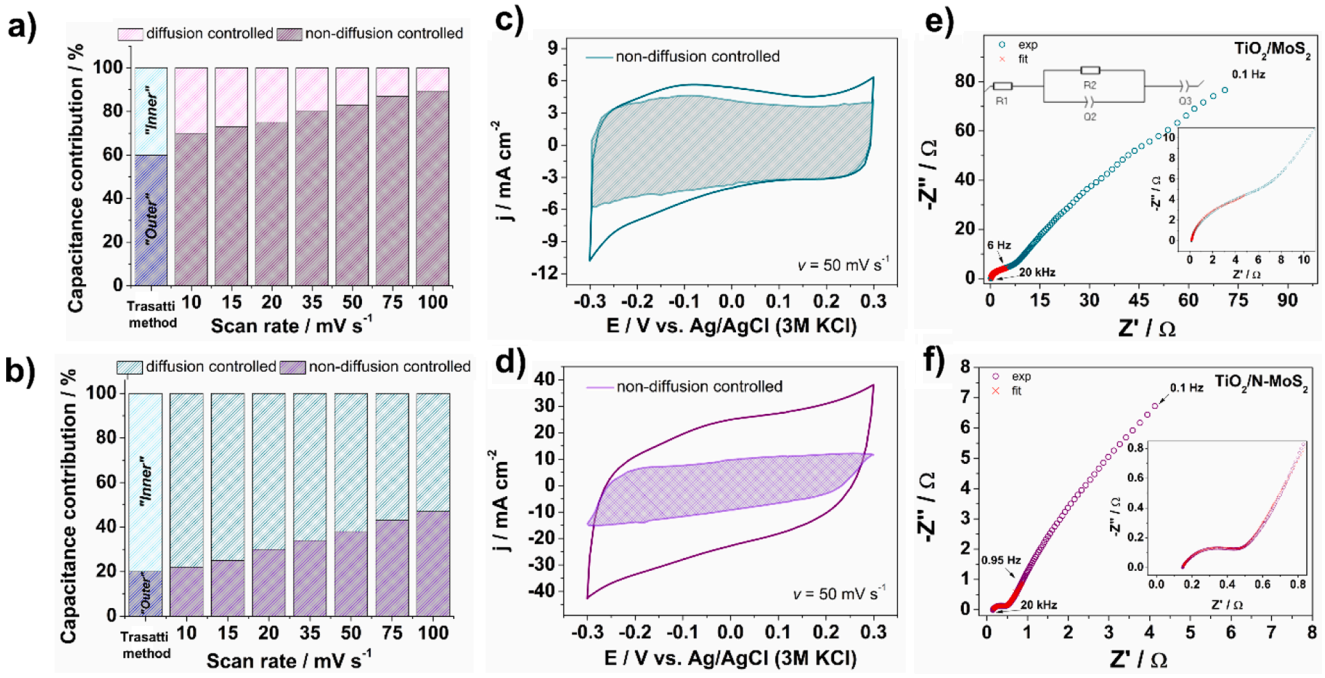

Fig. 8. Comparison of the contribution of the inner surface (and diffusion controlled), an outer surface (and non-diffusion controlled) capacitance calculated by Trasatti and Dunn's method, respectively, for a) TiO_2/MoS_2 (without ANI and APS) and b) for TiO_2/N-MoS_2 (with ANI and APS); CV curves for c) TiO_2/MoS_2 and d) TiO_2/N-MoS_2 with non-diffusion controlled capacitance contribution; EIS curves with electrical equivalent circuit used for both e) TiO_2/MoS_2 and f) TiO_2/N-MoS_2.

The results for the TiO_2/N-MoS_2 and TiO_2/MoS_2 electrode materials are presented in Fig. 8. The values obtained from Conway's analysis show that when ANI and APS were not present during the synthesis, the surface-confined processes have a major contribution to energy storage (Fig. 8**a**). Furthermore, Trasatti's approach also points out the enhanced contribution of the "outer" layer. On the other hand, when the introduction of nitrogen atoms was performed during the synthesis, mechanisms of energy storage changed significantly. For the TiO_2/N-MoS_2 electrode material, the "outer" layer contribution decreased to 20 % (according to the Trasatti method), and a similar dependence was observed for the results obtained from Dunn's approach (Fig. 8**b**), namely the diffusion of ions into the whole body of the material plays a major role in charge storage. An exemplary cyclic voltammetry curves for TiO_2/MoS_2 and TiO_2/N-MoS_2 with the calculated non-diffusion controlled processes contribution is presented in Fig. 8**c and 8d**. Such a transition from surface confinement to diffusion limitation may be observed when the path for ion transport lengthens due to the increase in layer thickness [81]. The comparison of the layers thickness is presented in **Figure S5**, and the results indicate that when the synthesis was performed with ANI and APS, the thickness of N-MoS_2 layer was increased (which thickness is around 1.8 μm in comparison with 0.6 μm). The electrode materials were also characterized by electrochemical impedance spectroscopy. The spectra of TiO_2/ MoS_2 and TiO_2/N-MoS_2 are presented in Fig. 8**e and 8f**. A semicircle may be distinguished in the high-frequency region of the spectra, and their diameter corresponds to the charge transfer resistance R_{ct} (R2). The decreased slope in the low-frequency region may indicate pseudocapacitive behavior [78,82]. Nevertheless, the electrode material that consists of differently obtained MoS_2 on the TiO_2 nanotubes is a very complex system and elaboration of the appropriate model is difficult to achieve. Thus, here the fragmentary analysis that covers only the high-frequency range was performed. The same electrical equivalent circuit (EEC) was applied for all spectra (shown in the inset of Fig. 8**e**), where Q stands for constant phase element (CPE). The results are shown in **Table S2**. R_e (R1) values that originate from the electrolyte and cable resistance are the same for both spectra (~0.147 Ω). As could be predicted from the shapes of the spectra, the R_{ct} for *N*-modified electrode material is lower (0.33 Ω) than for TiO_2/MoS_2 (5.27 Ω), suggesting that nitrogen atoms in the MoS_2 structure can significantly increase its conductivity [83]. The P value of CPE that corresponds to the capacitance of electrode material is much higher for TiO_2/N-MoS_2 which is in good agreement with cyclic voltammetry curves shown in Fig. 8**c and 8d**. Moreover, the n values are quite close to 1 (~0.91) for TiO_2/MoS_2 thus both CPEs act here almost as capacitors. The values of n for TiO_2/N-MoS_2 (0.73 and 0.78) suggest that diffusion-related phenomena may contribute to the CPEs used in the analysis which is in line with the results presented in Fig. 8**a and 8b**.

3.5. *Electrochemical measurements of N-MoS_2/TiO_2 electrode material in symmetric supercapacitor (SS)*

Finally, the TiO_2/N-MoS_2 electrode material was investigated in the symmetric two-electrode configuration in "coffee bag" construction. In order to determine the operating voltage window, cyclic voltammetry measurements were applied (see **Figure S6**). On this basis, the voltage value was fixed at 0.6 V, for which the galvanostatic charge–discharge tests at different current densities were performed. Regardless of the current density, only a small iR drop was observed during the discharge process in Fig. 9**a**. Moreover, as presented in Fig. 9**b**, the specific capacitance of 80 F g^{-1} was achieved at 3 A g^{-1}, as well as areal capacitance of 85 mF cm^{-2} at 2.6 mA cm^{-2}. The highest specific capacitance value, 140 F g^{-1}, was observed for the current density of 0.7 A g^{-1}. One of the crucial parameters for supercapacitors, which is long-term cycling stability, was also evaluated for the symmetrical device for the current density of 3 A g^{-1}, as displayed in Fig. 9**c**. The device was characterized by the initial specific capacitance of 76F g^{-1} and areal capacitance of 70 mF cm^{-2}, altogether with the capacitance retention of 84 % after 15 000 cycles. Taking SEM images allowed to establish that the electrode morphology did not change significantly, and that the nanostructures retained their spherical shape with nanosheet structures around them (see **Figure S7**). However, it was also observed that in some places the shell in the form of nanosheets has detached, which may have been one of the reasons for the decrease in capacitance after cycles. The superior electrochemical performance of the device was also confirmed by the coulombic efficiency of almost 100 % throughout the whole long-term cycling test (see Fig. 9**d**). Moreover, the triangle shape of chronopotentiometry curves before and after the cycles, presented in the inset of Fig. 9**d**, indicates that even after long-term measurements, the electrode material in the two-electrode configuration was

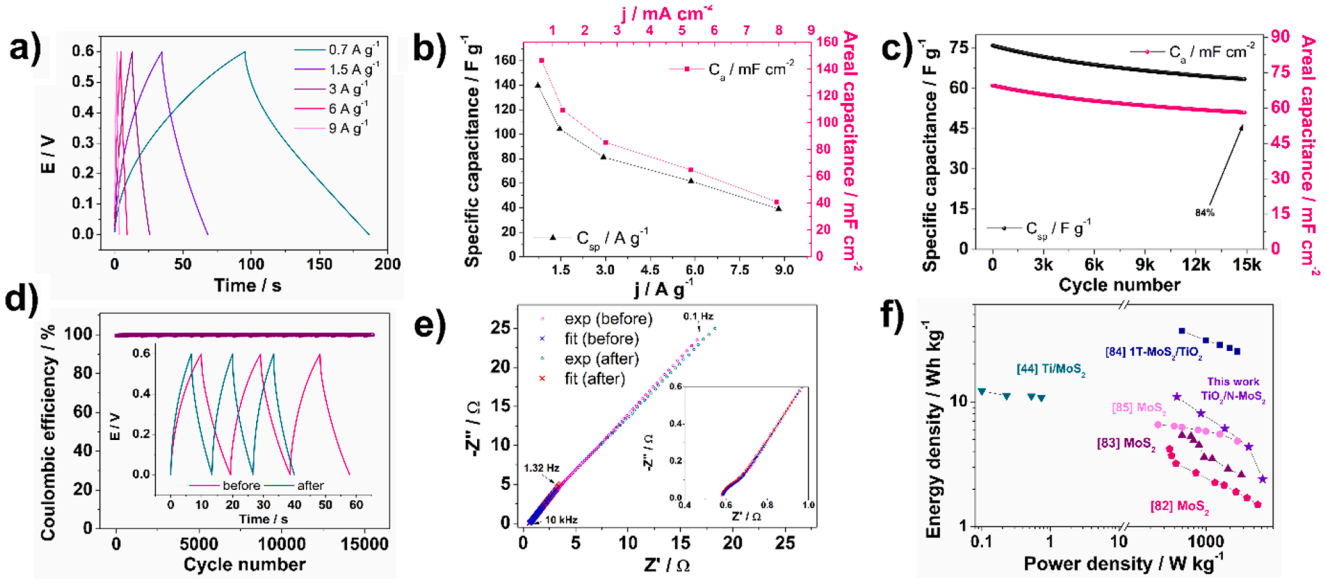

Fig. 9. a) GCD curves for different current densities for TiO_2/N-MoS_2 SS; b) Specific and areal capacitance the TiO_2/N-MoS_2 SS as a function of applied current density; c) Long-term cycling testing at 3 Ag-1; d) Coulombic efficiency during long-term cycling with the inset presenting GCD curves for the initial and final cycles at specific current of 3 Ag-1; e) experimental (o) and fitted with EEC (x) EIS data recorded before and after long-term cycling; f) Ragone plot with the results for TiO_2/N-MoS_2 SS compared with literature reports on MoS_2-based electrode materials.

characterized by capacitive properties, which is also consistent with EIS results (Fig. 9**e**). The analysis of the high-frequency range was performed using the same EEC as shown in Fig. 8**e**. The differences between the spectra recorded before and after the charge/discharge test are subtle, however, according to the fitting results a slight increase in charge transfer resistance with a simultaneous decrease in capacitance has been determined. The results are shown in **Table S2**. As shown in Fig. 9**f**, TiO_2/N-MoS_2 SS presented a maximum specific energy of 11.1 W kg^{-1} (at power density of 432.8 Wh kg^{-1}), and the highest specific power of 5193.4 Wh kg^{-1} (at specific energy of 2.4 W kg^{-1}) at high current density of 9 A g^{-1}, which is much higher in comparison with the literature results obtained for comparable current values [46,84–87]. Despite the fact that higher specific energy has been presented in some literature reports, it is highly likely to achieve such results also with the TiO_2/N-MoS_2 material, if used in an asymmetric construction.

4. Conclusions

In summary, the study focused on the synthesis of N-MoS_2 directly on a solid substrate of TiO_2 nanotubes using the hydrothermal method. The synthesis procedure was evaluated for the effect of hydrochloric acid, and on the basis of the results it was concluded that higher concentration promoted more effective synthesis of molybdenum sulfide. However, an excessive increase in HCl concentration led to both structure and morphology disruption of the TiO_2 substrate. The TiO_2/N-MoS_2 electrode material obtained with 0.5 M HCl was characterized by the highest areal capacitance value of 320 mF cm^{-2} and the most appropriate overall electrochemical performance for energy storage applications in general. Moreover, the influence of aniline monomer and ammonium persulfate during the synthesis was investigated. The results indicated that their addition not only significantly increased the crystallinity of the material, but also contributed to the enhanced capacitive properties. The reason for this was the introduction of nitrogen atoms into the structure of MoS_2, which also led to change in charge storage mechanism – from the surface confinement control, a major contribution was ascribed to diffusion controlled processes related to Faradaic capacitance. Finally, the symmetrical device constructed of two TiO_2/N-MoS_2 electrodes was characterized by the specific capacitance of specific capacitance of 76 F g^{-1} and areal capacitance of 70 mF cm^{-2}, with the superior coulombic efficiency and 84 % of capacitance retention after 15,000 cycles. Furthermore, the obtained values of energy and power density (11.1 W kg^{-1} and 5193.4 Wh kg^{-1}, respectively) indicate that the presented synthesis of MoS_2 directly on solid substrates may be an effective method for the preparation of electrode materials for high-power applications.

CRediT authorship contribution statement

Z. Zarach: Conceptualization, Data curation, Formal analysis, Investigation, Methodology, Validation, Visualization, Writing – original draft, Writing – review & editing. **A.P. Nowak:** Data curation, Formal analysis, Supervision, Validation, Writing – review & editing. **K. Trzciński:** Formal analysis, Methodology, Validation, Writing – review & editing. **G. Gajowiec:** Investigation, Resources. **G. Trykowski:** Investigation, Resources. **M. Sawczak:** Investigation, Resources. **M. Łapiński:** Investigation, Resources. **M. Szkoda:** Formal analysis, Funding acquisition, Methodology, Resources, Supervision, Validation, Writing – review & editing.

Declaration of Competing Interest

The authors declare the following financial interests/personal relationships which may be considered as potential competing interests: Mariusz Szkoda reports financial support was provided by National Centre for Research and Development.

Data availability

Data will be made available on request.

Acknowledgments

Funding: This work was supported by The National Centre for Research and Development (Grant no LIDER/15/0088/L-10/18/NCBR/2019).

Appendix A. Supplementary material

Supplementary data to this article can be found online at https://doi.org/10.1016/j.apsusc.2022.155187.

References

[1] C. Li, M.M. Islam, J. Moore, J. Sleppy, C. Morrison, K. Konstantinov, S.X. Dou, C. Renduchintala, J. Thomas, Wearable energy-smart ribbons for synchronous energy harvest and storage, Nat. Commun. 2016 71. 7 (2016) 1–10. 10.1038/ncomms13319.
[2] T.P. Narins, The battery business: Lithium availability and the growth of the global electric car industry, Extr. Ind. Soc. 4 (2017) 321–328, https://doi.org/10.1016/J.EXIS.2017.01.013.
[3] H. Marzougui, M. Amari, A. Kadri, F. Bacha, J. Ghouili, Energy management of fuel cell/battery/ultracapacitor in electrical hybrid vehicle, Int. J. Hydrogen Energy. 42 (2017) 8857–8869, https://doi.org/10.1016/J.IJHYDENE.2016.09.190.
[4] J. Pablo Esquivel, P. Alday, O.A. Ibrahim, B. Fernández, E. Kjeang, N. Sabaté, J. P. Esquivel, P. Alday, N. Sabaté, O.A. Ibrahim, E. Kjeang, B. Fernández, A Metal-Free and Biotically Degradable Battery for Portable Single-Use Applications, Adv. Energy Mater. 7 (2017) 1700275, https://doi.org/10.1002/AENM.201700275.
[5] S.W. Zhang, B.S. Yin, C. Liu, Z.B. Wang, D.M. Gu, A lightweight, compressible and portable sponge-based supercapacitor for future power supply, Chem. Eng. J. 349 (2018) 509–521, https://doi.org/10.1016/J.CEJ.2018.05.125.
[6] A. Scalia, F. Bella, A. Lamberti, S. Bianco, C. Gerbaldi, E. Tresso, C.F. Pirri, A flexible and portable powerpack by solid-state supercapacitor and dye-sensitized solar cell integration, J. Power Sources. 359 (2017) 311–321, https://doi.org/10.1016/J.JPOWSOUR.2017.05.072.
[7] S. Lv, L. Ma, X. Shen, H. Tong, Recent design and control of carbon materials for supercapacitors, J. Mater. Sci. 56 (2021) 1919–1942, https://doi.org/10.1007/S10853-020-05351-6/FIGURES/7.
[8] D.A.C. Brownson, D.K. Kampouris, C.E. Banks, An overview of graphene in energy production and storage applications, J. Power Sources. 196 (2011) 4873–4885, https://doi.org/10.1016/j.jpowsour.2011.02.022.
[9] A.K. Geim, K.S. Novoselov, The rise of graphene, in: Nanosci. Technol. A Collect. Rev. from Nat. Journals, World Scientific Publishing Co., 2009: pp. 11–19. 10.1142/9789814287005_0002.
[10] C.N.R. Rao, A.K. Sood, K.S. Subrahmanyam, A. Govindaraj, Graphene: The New Two-Dimensional Nanomaterial, Angew. Chemie Int. Ed. 48 (2009) 7752–7777, https://doi.org/10.1002/ANIE.200901678.
[11] B. Jache, P. Adelhelm, Use of Graphite as a Highly Reversible Electrode with Superior Cycle Life for Sodium-Ion Batteries by Making Use of Co-Intercalation Phenomena, Angew, Chemie. 126 (2014) 10333–10337, https://doi.org/10.1002/ANGE.201403734.
[12] Y. Sun, D. Chen, Z. Liang, Two-dimensional MXenes for energy storage and conversion applications, Mater. Today, Energy. 5 (2017) 22–36, https://doi.org/10.1016/J.MTENER.2017.04.008.
[13] B. Anasori, M.R. Lukatskaya, Y. Gogotsi, 2D metal carbides and nitrides (MXenes) for energy storage, Nat. Rev. Mater. 2017 22. 2 (2017) 1–17. 10.1038/natrevmats.2016.98.
[14] H.T. Tan, W. Sun, L. Wang, Q. Yan, 2D Transition Metal Oxides/Hydroxides for Energy-Storage Applications, ChemNanoMat 2 (2016) 562–577, https://doi.org/10.1002/CNMA.201500177.
[15] J. Li, Z. Liu, Q. Zhang, Y. Cheng, B. Zhao, S. Dai, H.H. Wu, K. Zhang, D. Ding, Y. Wu, M. Liu, M.S. Wang, Anion and cation substitution in transition-metal oxides nanosheets for high-performance hybrid supercapacitors, Nano Energy 57 (2019) 22–33, https://doi.org/10.1016/J.NANOEN.2018.12.011.
[16] R. Suresh Babu, R. Vinodh, A.L.F. de Barros, L.M. Samyn, K. Prasanna, M.A. Maier, C.H.F. Alves, H.J. Kim, Asymmetric supercapacitor based on carbon nanofibers as the anode and two-dimensional copper cobalt oxide nanosheets as the cathode, Chem. Eng. J. 366 (2019) 390–403, https://doi.org/10.1016/J.CEJ.2019.02.108.
[17] K.S. Ahn, R. Vinodh, B.G. Pollet, R.S. Babu, V. Ramkumar, S.C. Kim, K. Krishnakumar, H.J. Kim, A high-performance asymmetric supercapacitor consists of binder free electrode materials of bimetallic hydrogen phosphate (MnCo (HPO4)) hexagonal tubes and graphene ink, Electrochim. Acta. 426 (2022), 140763, https://doi.org/10.1016/J.ELECTACTA.2022.140763.
[18] G. Zhang, H. Liu, J. Qu, J. Li, Two-dimensional layered MoS 2: rational design, properties and electrochemical applications, Energy Environ. Sci. 9 (2016) 1190–1209, https://doi.org/10.1039/C5EE03761A.
[19] D. (David) Xia, F. Gong, X. Pei, W. Wang, H. Li, W. Zeng, M. Wu, D. V. Papavassiliou, Molybdenum and tungsten disulfides-based nanocomposite films for

energy storage and conversion: A review, Chem. Eng. J. 348 (2018) 908–928. 10.1016/J.CEJ.2018.04.207.
[20] Q. Ji, C. Li, J. Wang, J. Niu, Y. Gong, Z. Zhang, Q. Fang, Y. Zhang, J. Shi, L. Liao, X. Wu, L. Gu, Z. Liu, Y. Zhang, Metallic vanadium disulfide nanosheets as a platform material for multifunctional electrode applications, Nano Lett. 17 (2017) 4908–4916, https://doi.org/10.1021/ACS.NANOLETT.7B01914/ASSET/IMAGES/LARGE/NL-2017-01914V_0005.JPEG.
[21] M. Liu, Z. Wang, J. Liu, G. Wei, J. Du, Y. Li, C. An, J. Zhang, Synthesis of few-layer 1T′-MoTe 2 ultrathin nanosheets for high-performance pseudocapacitors, J. Mater. Chem. A. 5 (2017) 1035–1042, https://doi.org/10.1039/C6TA08206H.
[22] S. Yuan, S.Y. Pang, J. Hao, 2D transition metal dichalcogenides, carbides, nitrides, and their applications in supercapacitors and electrocatalytic hydrogen evolution reaction, Appl. Phys. Rev. 7 (2020), 021304, https://doi.org/10.1063/5.0005141.
[23] S. Liang, J. Zhou, J. Liu, A. Pan, Y. Tang, T. Chen, G. Fang, PVP-assisted synthesis of MoS 2 nanosheets with improved lithium storage properties, CrystEngComm 15 (2013) 4998–5002, https://doi.org/10.1039/C3CE40392K.
[24] Y. Zhang, W. Zeng, Y. Li, Hydrothermal synthesis and controlled growth of hierarchical 3D flower-like MoS2 nanospheres assisted with CTAB and their NO2 gas sensing properties, Appl. Surf. Sci. 455 (2018) 276–282, https://doi.org/10.1016/J.APSUSC.2018.05.224.
[25] S. Zhao, G. Wang, J. Liao, S. Lv, Z. Zhu, Z. Li, Vertically aligned MoS2/ZnO nanowires nanostructures with highly enhanced NO2 sensing activities, Appl. Surf. Sci. 456 (2018) 808–816, https://doi.org/10.1016/J.APSUSC.2018.06.103.
[26] C. Zhang, H. Bin Wu, Z. Guo, X.W. Lou, Facile synthesis of carbon-coated MoS2 nanorods with enhanced lithium storage properties, Electrochem. Commun. 20 (2012) 7–10, https://doi.org/10.1016/J.ELECOM.2012.03.039.
[27] M. Wang, G. Li, H. Xu, Y. Qian, J. Yang, Enhanced lithium storage performances of hierarchical hollow MoS 2 nanoparticles assembled from nanosheets, ACS Appl. Mater. Interfaces. 5 (2013) 1003–1008, https://doi.org/10.1021/AM3026954/SUPPL_FILE/AM3026954_SI_001.PDF.
[28] M. Li, A. Addad, Y. Zhang, A. Barras, P. Roussel, M.A. Amin, S. Szunerits, R. Boukherroub, Flower-like Nitrogen-co-doped MoS2@RGO Composites with Excellent Stability for Supercapacitors, ChemElectroChem. 8 (2021) 2903–2911, https://doi.org/10.1002/CELC.202100401.
[29] Y. Chao, Y. Ge, Z. Chen, X. Cui, C. Zhao, C. Wang, G.G. Wallace, One-Pot Hydrothermal Synthesis of Solution-Processable MoS2/PEDOT:PSS Composites for High-Performance Supercapacitors, ACS Appl. Mater. Interfaces. 13 (2021) 7285–7296, https://doi.org/10.1021/ACSAMI.0C21439/ASSET/IMAGES/LARGE/AM0C21439_0007.JPEG.
[30] D. Cao, Q. Wang, S. Zhu, X. Zhang, Y. Li, Y. Cui, Z. Xue, S. Gao, Hydrothermal construction of flower-like MoS2 on TiO2 NTs for highly efficient environmental remediation and photocatalytic hydrogen evolution, Sep. Purif. Technol. 265 (2021), 118463, https://doi.org/10.1016/J.SEPPUR.2021.118463.
[31] W.J. Li, E.W. Shi, J.M. Ko, Z.Z. Chen, H. Ogino, T. Fukuda, Hydrothermal synthesis of MoS2 nanowires, J. Cryst. Growth. 250 (2003) 418–422, https://doi.org/10.1016/S0022-0248(02)02412-0.
[32] W.H. Hu, G.Q. Han, F.N. Dai, Y.R. Liu, X. Shang, B. Dong, Y.M. Chai, Y.Q. Liu, C. G. Liu, Effect of pH on the growth of MoS2 (002) plane and electrocatalytic activity for HER, Int. J. Hydrogen Energy. 41 (2016) 294–299, https://doi.org/10.1016/J.IJHYDENE.2015.09.076.
[33] Z. Xiong, G. Zhu, H. Wu, G. Shi, P.u. Xu, H. Yi, Y. Mao, B. Wang, X. Yu, Hydrochloric Acid-Assisted Synthesis of Highly Dispersed MoS2Nanoflowers as the Cathode Material for Mg-Li Batteries, ACS Appl. Energy Mater. 5 (5) (2022) 6274–6281.
[34] P. Wang, H. Sun, Y. Ji, W. Li, X. Wang, P. Wang, Y. Ji, W. Li, X. Wang, H. Sun, Three-Dimensional Assembly of Single-Layered MoS2, Adv. Mater. 26 (2014) 964–969, https://doi.org/10.1002/ADMA.201304120.
[35] F. Huang, R. Meng, Y. Sui, F. Wei, J. Qi, Q. Meng, Y. He, One-step hydrothermal synthesis of a CoS2@MoS2 nanocomposite for high-performance supercapacitors, J. Alloys Compd. 742 (2018) 844–851, https://doi.org/10.1016/J.JALLCOM.2018.01.324.
[36] Y. Cai, H. Kang, F. Jiang, L. Xu, Y. He, J. Xu, X. Duan, W. Zhou, X. Lu, Q. Xu, The construction of hierarchical PEDOT@MoS2 nanocomposite for high-performance supercapacitor, Appl. Surf. Sci. 546 (2021), 149088, https://doi.org/10.1016/J.APSUSC.2021.149088.
[37] J. Wang, L. Sun, Y. Gong, L. Wu, C. Sun, X. Zhao, X. Shi, Y. Lin, K. Wang, Y. Zhang, A CNT/MoS2@PPy composite with double electron channels and boosting charge transport for high-rate lithium storage, Appl. Surf. Sci. 566 (2021), 150693, https://doi.org/10.1016/J.APSUSC.2021.150693.
[38] P. Sun, R. Wang, Q. Wang, H. Wang, X. Wang, Uniform MoS2 nanolayer with sulfur vacancy on carbon nanotube networks as binder-free electrodes for asymmetrical supercapacitor, Appl. Surf. Sci. 475 (2019) 793–802, https://doi.org/10.1016/J.APSUSC.2019.01.007.
[39] S. Zhang, R. Hu, P. Dai, X. Yu, Z. Ding, M. Wu, G. Li, Y. Ma, C. Tu, Synthesis of rambutan-like MoS2/mesoporous carbon spheres nanocomposites with excellent performance for supercapacitors, Appl. Surf. Sci. 396 (2017) 994–999, https://doi.org/10.1016/J.APSUSC.2016.11.074.
[40] B. Kirubasankar, M. Narayanasamy, J. Yang, M. Han, W. Zhu, Y. Su, S. Angaiah, C. Yan, Construction of heterogeneous 2D layered MoS2/MXene nanohybrid anode material via interstratification process and its synergetic effect for asymmetric supercapacitors, Appl. Surf. Sci. 534 (2020), 147644, https://doi.org/10.1016/J.APSUSC.2020.147644.
[41] M.G. Fayed, S.Y. Attia, Y.F. Barakat, E.E. El-Shereafy, M.M. Rashad, S.G. Mohamed, Carbon and nitrogen co-doped MoS2 nanoflakes as an electrode material for lithium-ion batteries and supercapacitors, Sustain. Mater. Technol. 29 (2021) e00306.
[42] P. Tang, J. Jiao, Q. Fan, X. Wang, V. Agrawal, Q. Xu, Interlayer spacing engineering in N doped MoS2 for efficient lithium ion storage, Mater. Chem. Phys. 261 (2021), 124166, https://doi.org/10.1016/J.MATCHEMPHYS.2020.124166.
[43] I.T. Bello, K.O. Otun, G. Nyongombe, O. Adedokun, G.L. Kabongo, M.S. Dhlamini, Non-modulated synthesis of cobalt-doped MoS2 for improved supercapacitor performance, Int. J. Energy Res. 46 (2022) 8908–8918, https://doi.org/10.1002/ER.7765.
[44] J. Shao, Y. Li, M. Zhong, Q. Wang, X. Luo, K. Li, W. Zhao, Enhanced-performance flexible supercapacitor based on Pt-doped MoS2, Mater. Lett. 252 (2019) 173–177, https://doi.org/10.1016/J.MATLET.2019.05.124.
[45] D. Vikraman, S. Hussain, K. Karuppasamy, A. Kathalingam, E.B. Jo, A. Sanmugam, J. Jung, H.S. Kim, Engineering the active sites tuned MoS2 nanoarray structures by transition metal doping for hydrogen evolution and supercapacitor applications, J. Alloys Compd. 893 (2022), 162271, https://doi.org/10.1016/J.JALLCOM.2021.162271.
[46] L. Wang, Y. Ma, M. Yang, Y. Qi, Titanium plate supported MoS2 nanosheet arrays for supercapacitor application, Appl. Surf. Sci. 396 (2017) 1466–1471, https://doi.org/10.1016/J.APSUSC.2016.11.193.
[47] K. Krishnamoorthy, G.K. Veerasubramani, P. Pazhamalai, S.J. Kim, Designing two dimensional nanoarchitectured MoS2 sheets grown on Mo foil as a binder free electrode for supercapacitors, Electrochim. Acta. 190 (2016) 305–312, https://doi.org/10.1016/J.ELECTACTA.2015.12.148.
[48] J.M. Soon, K.P. Loh, Electrochemical double-layer capacitance of MoS2 nanowall films, Electrochem. Solid-State Lett. 10 (2007) 250–254, https://doi.org/10.1149/1.2778851/XML.
[49] N. Choudhary, M. Patel, Y.H. Ho, N.B. Dahotre, W. Lee, J.Y. Hwang, W. Choi, Directly deposited MoS 2 thin film electrodes for high performance supercapacitors, J. Mater. Chem. A. 3 (2015) 24049–24054, https://doi.org/10.1039/C5TA08095A.
[50] M. Szkoda, K. Siuzdak, A. Lisowska-Oleksiak, Optimization of electrochemical doping approach resulting in highly photoactive iodine-doped titania nanotubes, J. Solid State Electrochem. 20 (2016) 563–569, https://doi.org/10.1007/S10008-015-3081-7/FIGURES/7.
[51] G. Woo An, L.K. Dhandole, H. Park, H. Sub Bae, M.A. Mahadik, J. Suk Jang, Enhanced Charge Transfer Process in Morphology Restructured TiO2 Nanotubes via Hydrochloric Acid Assisted One Step In-Situ Hydrothermal Approach, ChemCatChem 11 (2019) 5606–5614, https://doi.org/10.1002/CCTC.201901177.
[52] H. Zhang, P. Zhou, Z. Chen, W. Song, H. Ji, W. Ma, C. Chen, J. Zhao, Hydrogen-Bond Bridged Water Oxidation on 001 Surfaces of Anatase TiO2, J. Phys. Chem. C. 121 (2017) 2251–2257, https://doi.org/10.1021/ACS.JPCC.6B11900/ASSET/IMAGES/LARGE/JP-2016-11900P_0004.JPEG.
[53] T.D. Nguyen Phan, H.D. Pham, T. Viet Cuong, E. Jung Kim, S. Kim, E. Woo Shin, A simple hydrothermal preparation of TiO2 nanomaterials using concentrated hydrochloric acid, J. Cryst. Growth. 312 (2009) 79–85, https://doi.org/10.1016/J.JCRYSGRO.2009.09.032.
[54] Q.Q. Fan, Z.Y. Qin, X. Liang, L. Li, W.H. Wu, M.F. Zhu, Reducing defects on multi-walled carbon nanotube surfaces induced by low-power ultrasonic-assisted hydrochloric acid treatment, Http://Dx.Doi.Org/10.1080/17458080903536541. 5 (2010) 337–347, https://doi.org/10.1080/17458080903536541.
[55] G. Feng, A. Wei, Y. Zhao, J. Liu, Synthesis of flower-like MoS2 nanosheets microspheres by hydrothermal method, J. Mater. Sci. Mater. Electron. 26 (2015) 8160–8166, https://doi.org/10.1007/S10854-015-3476-3/FIGURES/6.
[56] K. Trzciński, M. Szkoda, Z. Zarach, M. Sawczak, A.P. Nowak, Towards spectroscopic monitoring of photoelectrodes: In-situ Raman photoelectrochemistry of a TiO2/prussian blue photoanode, Electrochim. Acta. 404 (2022), 139774, https://doi.org/10.1016/J.ELECTACTA.2021.139774.
[57] M. Wtulich, M. Szkoda, G. Gajowiec, M. Gazda, K. Jurak, M. Sawczak, A. Lisowska-Oleksiak, Hydrothermal Cobalt Doping of Titanium Dioxide Nanotubes towards Photoanode Activity Enhancement, Mater. 2021, Vol. 14, Page 1507. 14 (2021) 1507. 10.3390/MA14061507.
[58] N.T. Tung, D.N. Huyen, Effect of HCl on the Formation of TiO2 Nanocrystallites, J. Nanomater. 2016 (2016), https://doi.org/10.1155/2016/6547271.
[59] D. Sarkar, D. Das, S. Das, A. Kumar, S. Patil, K.K. Nanda, D.D. Sarma, A. Shukla, Expanding Interlayer Spacing in MoS2 for Realizing an Advanced Supercapacitor, ACS Energy Lett. 4 (2019) 1602–1609, https://doi.org/10.1021/ACSENERGYLETT.9B00983/SUPPL_FILE/NZ9B00983_SI_001.PDF.
[60] M. Chen, B. Ji, Z. Dai, X. Du, B. He, G. Chen, D. Liu, S. Chen, K.H. Lo, S. Wang, B. Zhou, H. Pan, Vertically-aligned 1T/2H-MS2 (M = Mo, W) nanosheets for surface-enhanced Raman scattering with long-term stability and large-scale uniformity, Appl. Surf. Sci. 527 (2020), 146769, https://doi.org/10.1016/J.APSUSC.2020.146769.
[61] Z. Zhang, Y. Dong, G. Liu, J. Li, H. Sun, H. Luo, S. Liu, The ultrafine monolayer 1 T/2H-MoS2: Preparation, characterization and amazing photocatalytic characteristics, Colloids Surfaces A Physicochem. Eng. Asp. 589 (2020), 124431, https://doi.org/10.1016/J.COLSURFA.2020.124431.
[62] Y. Qi, Q. Xu, Y. Wang, B. Yan, Y. Ren, Z. Chen, CO2-Induced Phase Engineering: Protocol for Enhanced Photoelectrocatalytic Performance of 2D MoS2 Nanosheets, ACS Nano 10 (2016) 2903–2909, https://doi.org/10.1021/ACSNANO.6B00001/SUPPL_FILE/NN6B00001_SI_001.PDF.
[63] M. Hou, Y. Qiu, G. Yan, J. Wang, D. Zhan, X. Liu, J. Gao, L. Lai, Aging mechanism of MoS2 nanosheets confined in N-doped mesoporous carbon spheres for sodium-ion batteries, Nano Energy 62 (2019) 299–309, https://doi.org/10.1016/J.NANOEN.2019.05.048.
[64] I.H. Kwak, I.S. Kwon, H.G. Abbas, J. Seo, G. Jung, Y. Lee, D. Kim, J.P. Ahn, J. Park, H.S. Kang, Intercalated complexes of 1T′-MoS 2 nanosheets with alkylated

phenylenediamines as excellent catalysts for electrochemical hydrogen evolution, J. Mater. Chem. A. 7 (2019) 2334–2343, https://doi.org/10.1039/C8TA11085A.
[65] O.M. Peeters, E.A. Butler, D.G. Peters, E.H. Swift, Pathways in thioacetamide hydrolysis in aqueous acid: detection by kinetic analysis, J. Chem. Soc. Perkin Trans. 2 (1974) 1832–1835, https://doi.org/10.1039/P29740001832.
[66] E.A. Butler, D.G. Peters, E.H. Swift, Hydrolysis Reactions of Thioacetamide in Aqueous Solutions, Anal. Chem. 30 (1958) 1379–1383, https://doi.org/10.1021/AC60140A027/ASSET/AC60140A027.FP.PNG_V03.
[67] D. Rosenthal, T.I. Taylor, A Study of the Mechanism and Kinetics of the Thioacetamide Hydrolysis Reaction, J. Am. Chem. Soc. 79 (1957) 2684–2690, https://doi.org/10.1021/JA01568A007/ASSET/JA01568A007.FP.PNG_V03.
[68] S.M. Senthil Kumar, K. Selvakumar, R. Thangamuthu, A. Karthigai Selvi, S. Ravichandran, G. Sozhan, K. Rajasekar, N. Navascues, S. Irusta, Hydrothermal assisted morphology designed MoS2 material as alternative cathode catalyst for PEM electrolyser application, Int. J. Hydrogen Energy. 41 (2016) 13331–13340, https://doi.org/10.1016/J.IJHYDENE.2016.05.285.
[69] K. Matsui, H. Suzuki, M. Ohgai, H. Arashi, Raman Spectroscopic Studies on the Formation Mechanism of Hydrous-Zirconia Fine Particles, J. Am. Ceram. Soc. 78 (1995) 146–152, https://doi.org/10.1111/J.1151-2916.1995.TB08374.X.
[70] Y. Li, H. Li, L. Tian, Q. Wang, F. Wu, F. Zhang, L. Du, Y. Huang, Vertical phase segregation suppression for efficient FA-based quasi-2D perovskite solar cells via HCl additive, J. Mater. Sci. Mater. Electron. 31 (2020) 12301–12308, https://doi.org/10.1007/S10854-020-03775-Z/FIGURES/7.
[71] C. Yang, Z. Chen, I. Shakir, Y. Xu, H. Lu, Rational synthesis of carbon shell coated polyaniline/MoS2 monolayer composites for high-performance supercapacitors, Nano Res. 2016 94. 9 (2016) 951–962. 10.1007/S12274-016-0983-3.
[72] J. Chao, L. Yang, J. Liu, R. Hu, M. Zhu, Sandwiched MoS2/polyaniline nanosheets array vertically aligned on reduced graphene oxide for high performance supercapacitors, Electrochim. Acta. 270 (2018) 387–394, https://doi.org/10.1016/J.ELECTACTA.2018.03.072.
[73] S. Zhang, X. Song, S. Liu, F. Sun, G. Liu, Z. Tan, Template-assisted synthesized MoS2/polyaniline hollow microsphere electrode for high performance supercapacitors, Electrochim. Acta. 312 (2019) 1–10, https://doi.org/10.1016/J.ELECTACTA.2019.04.177.
[74] E. Ghaleghafi, M.B. Rahmani, Exploring different routes for the synthesis of 2D MoS2/1D PANI nanocomposites and investigating their electrical properties, Phys. E Low-Dimensional Syst. Nanostructures. 138 (2022), 115128, https://doi.org/10.1016/J.PHYSE.2021.115128.
[75] J. Dai, S. Zeng, Y. Lv, H. Xie, L. Luo, Y. Xu, L. Dai, A facile strategy for tailoring polyaniline by MoS2 nanosheets to obtain excellent electrochemical properties, Electrochim. Acta. 378 (2021), 138149, https://doi.org/10.1016/J.ELECTACTA.2021.138149.
[76] H. Ganesha, S. Veeresh, Y.S. Nagaraju, M. Vandana, S.P. Ashokkumar, H. Vijeth, H. Devendrappa, Growth of 3-Dimentional MoS2-PANI nanofiber for high electrochemical performance, Mater. Res. Express. 7 (2020), https://doi.org/10.1088/2053-1591/ab9e30.
[77] Z. Zarach, K. Trzciński, M. Łapiński, A. Lisowska-Oleksiak, M. Szkoda, Improving the Performance of a Graphite Foil/Polyaniline Electrode Material by a Thin PEDOT:PSS Layer for Application in Flexible, High Power Supercapacitors, Mater. 2020, Vol. 13, Page 5791. 13 (2020) 5791. 10.3390/MA13245791.
[78] G.Z. Chen, Linear and non-linear pseudocapacitances with or without diffusion control, Prog. Nat. Sci. Mater. Int. 31 (2021) 792–800, https://doi.org/10.1016/J.PNSC.2021.10.011.
[79] S. Ardizzone, G. Fregonara, S. Trasatti, "Inner" and "outer" active surface of RuO2 electrodes, Electrochim. Acta. 35 (1990) 263–267, https://doi.org/10.1016/0013-4686(90)85068-X.
[80] T.-C. Liu, W.G. Pell, B.E. Conway, S.L. Roberson, Behavior of Molybdenum Nitrides as Materials for Electrochemical Capacitors: Comparison with Ruthenium Oxide, J. Electrochem. Soc. 145 (1998) 1882–1888, https://doi.org/10.1149/1.1838571/XML.
[81] G.A. Snook, C. Peng, D.J. Fray, G.Z. Chen, Achieving high electrode specific capacitance with materials of low mass specific capacitance: Potentiostatically grown thick micro-nanoporous PEDOT films, Electrochem. Commun. 9 (2007) 83–88, https://doi.org/10.1016/j.elecom.2006.08.037.
[82] R. Yuksel, O. Buyukcakir, P.K. Panda, S.H. Lee, Y. Jiang, D. Singh, S. Hansen, R. Adelung, Y.K. Mishra, R. Ahuja, R.S. Ruoff, Necklace-like Nitrogen-Doped Tubular Carbon 3D Frameworks for Electrochemical Energy Storage, Adv. Funct. Mater. 30 (2020) 1909725, https://doi.org/10.1002/ADFM.201909725.
[83] C. Lu, L. Yang, B. Yan, L. Sun, P. Zhang, W. Zhang, Z. Sun, C. Lu, L. Yang, B. Yan, P. Zhang, W. Zhang, Z.M. Sun, L. Sun, Nitrogen-Doped Ti3C2 MXene: Mechanism Investigation and Electrochemical Analysis, Adv. Funct. Mater. 30 (2020) 2000852, https://doi.org/10.1002/ADFM.202000852.
[84] B.A. Ali, A.M.A. Omar, A.S.G. Khalil, N.K. Allam, Untapped Potential of Polymorph MoS2: Tuned Cationic Intercalation for High-Performance Symmetric Supercapacitors, ACS Appl. Mater. Interfaces. 11 (2019) 33955–33965, https://doi.org/10.1021/ACSAMI.9B11444/ASSET/IMAGES/LARGE/AM9B11444_0007.JPEG.
[85] R.K. Mishra, M. Krishnaih, S.Y. Kim, A.K. Kushwaha, S.H. Jin, Binder-free, scalable hierarchical MoS2 as electrode materials in symmetric supercapacitors for energy harvesting applications, Mater. Lett. 236 (2019) 167–170, https://doi.org/10.1016/J.MATLET.2018.10.009.
[86] J. Zhou, M. Guo, L. Wang, Y. Ding, Z. Zhang, Y. Tang, C. Liu, S. Luo, 1T-MoS2 nanosheets confined among TiO2 nanotube arrays for high performance supercapacitor, Chem. Eng. J. 366 (2019) 163–171, https://doi.org/10.1016/J.CEJ.2019.02.079.
[87] D. Kesavan, V.K. Mariappan, P. Pazhamalai, K. Krishnamoorthy, S.J. Kim, Topochemically synthesized MoS2 nanosheets: A high performance electrode for wide-temperature tolerant aqueous supercapacitors, J. Colloid Interface Sci. 584 (2021) 714–722, https://doi.org/10.1016/J.JCIS.2020.09.088.